ACS APPLIED MATERIALS & INTERFACES

LETTER

www.acsami.org

Solution Fabrication and Photoelectrical Properties of $CuInS_2$ Nanocrystals on TiO_2 Nanorod Array

Zheng-ji Zhou, Jun-qi Fan, Xia Wang, Wei-zhong Sun, Wen-hui Zhou, Zu-liang Du, and Si-xin Wu*

Key Lab for Special Functional Materials of Ministry of Education, Henan University, Kaifeng 475004, China

Supporting Information

ABSTRACT: One-dimensional semiconductor architectures are receiving attention in preparing photovoltaic solar cells because of its superior charge transport as well as excellent light-harvesting efficiency. In this study, vertically aligned single-crystalline TiO_2 nanorods array was grown directly on transparent conductive glass (FTO), and then $CuInS_2$ nanocrystals were deposited on nanorods array by spin coating method to form $TiO_2/CuInS_2$ heterostructure films. The resulting nanostructure assembly and composition was confirmed by field-emission scanning electron microscope (FESEM) , transmission electron microscopy (TEM), high-resolution TEM, and X-ray diffraction(XRD). Ultraviolet-visible absorption spectroscopy (UV−vis) data indicates that the absorbance of the nanocomposite film extended into the visible region compared with bare TiO_2 nanorod arrays. The surface photovoltage spectra (SPS) also showed a new and enhanced response region corresponding to the absorption spectrum. These results suggest that the novel $CuInS_2$ nanocrystals sensitized TiO_2 nanorod array on FTO photoelectrodes has a potential application in photovoltaic devices.

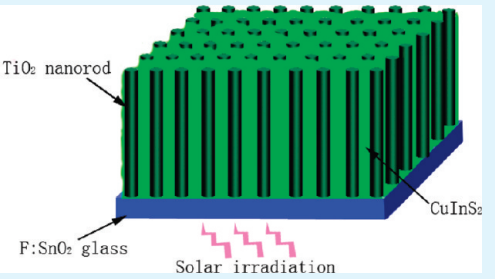

KEYWORDS: TiO_2, nanorod arrays, $CuInS_2$ nanocrystals, photoelectrodes, photovoltage

1. INTRODUCTION

TiO_2 is one of the most significant semiconductor materials extensively used in the field of photovoltaic and photocatalytic because of its high chemical stability, a long lifetime of photon-generated carriers and strong catalytic activity.[1−7] However, the energy conversion efficiency of TiO_2 is low, which is mainly because TiO_2 has a large band gap about 3.2 eV and absorbs solar light only in the ultraviolet region,[8,9] which comprises a small portion (approximately 5%) of the solar spectrum.[10] For extending the spectral response into the region of visible, many kinds of method have been developed, of which dye-sensitized[11−14] and quantum-dot-sensitized[15−18] TiO_2 photoelectrodes are two strategies generally used by researchers. But organic dye has disadvantages such as high cost, short age, and unstable performance.[19,20] Now, much attention has been focused on using inorganic short band-gap semiconductor to substitute organic dye.[21−23] Among the inorganic semiconductors materials, $CuInS_2$ (CIS) is a very promising candidate for its direct band gap of 1.50 eV, which is closely matched to the best band gap of the solar cell materials (1.45 eV),[24] having high absorption coefficient of 1×10^5 $cm^{-1}$and environmentally benign material with no toxic composition,[25] as well as the n-type or p-type conductivity of $CuInS_2$ can be easily adjusted by controlling the molar ratio of the compositional elements.[26] Thus, developing a simple method to deposit $CuInS_2$ onto TiO_2 is very significant.

Actually, A. Goossens and coworks have done many research works on deposition $CuInS_2$ inside a nanoporous matrix of TiO_2 by atomic layer chemical vapor deposition and spray pyrolysis to form so-called 3D-solar cell.[27−29] Compared to the disordered nanoporous matrix, One-dimensional(1D) ordered TiO_2 nanostructures offer direct electrical pathways for photogenerated electrons, which ensure efficient separation and collection of all charge carriers.[30−33] Furthermore, 1D nanostructures array films also bear unique advantages of low reflectance.[34] Therefore, fabrication of 1D TiO_2 nanostructures framework for light harvesting $CuInS_2$ can not only increase the charge transport rate but also provide superior optical adsorption properties, which are two crucial factors in photoelectrochemical device.

In this work, we present a simple solution-processed method to prepare $CuInS_2$ nanocrystals sensitized single-crystalline TiO_2 nanorod array on FTO photoelectrodes. This approach applied the TiO_2 nanorod array which was grown directly on FTO substrate via hydrothermal reaction and allowed $CuInS_2$ nanocrystals to infiltrate the interspace of TiO_2 nanorod array by spin-coating, using inorganic Cu and In salts and thiourea served as the precursor solution. In the obtained structure, wide bandgap n-type semiconductor TiO_2 nanorods array and p-type visible light sensitive semiconductor $CuInS_2$ nanocrystals are mixed together to form a nanometerscale interpenetrating network (Figure 1). UV−vis absorption spectra and SPS indicate the as-prepared photoelectrodes have excellent visible light absorbing ability and electron separation and transport properties. At the same time, to examine the impact of structure factors on photoelectrical properties of the complex films, we have

Received: April 22, 2011
Accepted: June 20, 2011
Published: June 20, 2011

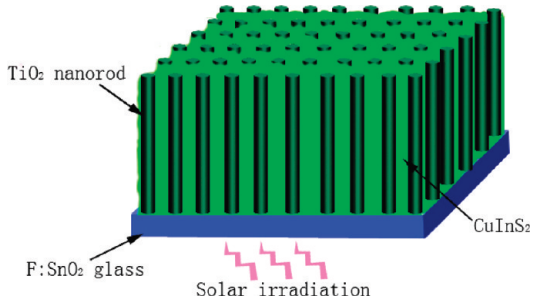

Figure 1. Schematic of the $CuInS_2$ deposited on TiO_2 nanorod.

performed different $CuInS_2$ deposition cycles to optimize the parametric of the photoelectrodes.

2. EXPERIMENTAL SECTION

2.1. Materials. Titanium butoxide, $In(OAc)_3$, CuI, thiourea, 1-butylamine, and 1-propionic acid were purchased from Sigma-Aldrich China, concentrated hydrochloric acid (36.5%-38% by weight) was purchased from Tianjin Chemical Reagents Co.. All the reagents were used without further purification. Triply-deionized water (resistivity of 18.2 MΩ cm^{-1}) was obtained from Milli-Q ultra-pure water system-(Millipore, USA). FTO coated glass slides (F: SnO_2, 14 Ω/square, Nippon Sheet Glass Group, Japan) were thoroughly washed with a mixed solution of deionized water, acetone, and 2-propanol (volume rations of 1:1:1) under sonication for 60 min.

2.2. TiO_2 Nanorod Array Synthesis. The experimental details of the synthesis procedure for preparing TiO_2 nanorod array can be found in Liu et al.[35] In a typical experiment, 30 mL of deionized water was mixed with 30 mL of concentrated hydrochloric acid in a Teflon-lined stainless steel autoclave followed by stirring at ambient condition for 5 min, then 1 mL of titanium butoxide was added to the mixture. After it was stirred for another 5 min, one piece of FTO substrate was placed at an angle against the wall of the Teflon reactor with the conductive side facing down. The hydrothermal synthesis was conducted at 150°C for 20 h in an electric oven. After synthesis, the autoclave was cooled to room temperature under flowing water, the FTO substrate was taken out, rinsed extensively with distilled water and dried in ambient air.

2.3. $CuInS_2$ Nanocrystals Deposition on TiO_2 Nanorod Array. $CuInS_2$ nanocrystals were deposited on TiO_2 nanorods through a spin-coating method similar to that described by Moses et al.[36] Briefly, 0.1 mmol $In(OAc)_3$, 0.11 mmol CuI, and 0.5 mmol thiourea were mixed with 0.6 mL of 1-butylamine and 40 μL of 1-propionic acid followed by shaken for 1 min. The CIS precursor solution was then spin-cast onto the TiO_2 nanorod array substrates at 1300 rpm for 30 s, finally, the obtained sample was calcined at 150°C for 10 min and then heated to 250°C at a rate of 10°C/min and held another 10 min at this temperature, all the experiment was finished under an inert atmosphere in a glovebox. Such a spin-cast course was repeated several times until the interspace of the nanorod arrays was infilled. To increase the crystallinity of $CuInS_2$ as well as the contact between $CuInS_2$ nanocrystals and TiO_2 nanorod at the interface, a subsequent annealing process of the sample in sulfur ambiance at 500°C for 30 min was implemented.

2.4. Characterization. The morphology of the as-prepared sample was studied by a field-emission gun scanning electron microscope (JSM-7001F, 10 KV). The crystal structure was determined by X-ray diffraction (XRD). The XRD patterns were recorded by using a Philips X'Pert PRO X-ray diffractometer with Cu Kα1 radiation (λ = 1.5406 Å) from 20 to 70° at a scanning rate of 2.4° min^{-1}. X-ray tube voltage and current were set at 40 kV and 40 mA, repectively. Transmission electron microscopy (TEM) and high-resolution TEM (HRTEM) investigations were carried out by a JEOL JEM-2100(UHR) microscope with a digital camera. The nanocomposites were detached from the FTO substrate, then dispersed in ethanol by sonication, and dropped onto a carbon film supported on a copper grid. Energy-dispersive spectroscopy (EDS) equipped on SEM was used to analyze the composition of the structure. The optical properties were examined by UV-visible spectroscopy (UNICAM HEλIOSαUVvisible-NIR spectrometer). Photogenerated charge separation and transfer performance of the photoelectrodes was evaluated through the surface photovoltage spectrum (SPS), which was measured on homemade SPS equipment. Monochromatic light was obtained by passing light from a 500 W xenon lamp through a monochromator. A lock-in amplifier (SR830-DSP, made in the USA) synchronized with a light chopper was employed to amplify the photovoltage signal. The spectral resolution was 1 nm.

3. RESULTS AND DISCUSSION

3.1. Characterization of $CuInS_2$ Nanocrystals -Sensitized TiO_2 Nanorod Array. Figure 2 shows the field-emission scanning electron microscopy images of the highly ordered, single-crystalline rutile TiO_2 nanorod array on FTO substrates and the $CuInS_2$ nanocrystals deposited onto the TiO_2 nanorods electrode by different spin-cast cycle. As shown in Figure 2A, The entire surface of the FTO substrate is covered very uniformly with TiO_2 nanorods. Figure 2B is a high magnification of the TiO_2 array, showing that the nanorods are tetragonal in shape with square top facets, which is the expected growth habit for the tetragonal crystal structure. From the cross-sectional view of the sample, we can see that the well aligned nanorods are nearly vertically on the FTO substrate. After 20 h of growth, the average length of nanorods is 3μm (see the Supporting Information, SI-1).

Figure 2C−H displays TiO_2 nanorod arrays coated with $CuInS_2$ nanocrystals for different cycles from 5, 10, and 20. The gap in the nanorod arrays was slowly infilled by $CuInS_2$ nanocrystals with the increase in spin coating cycles. After 20 cycles of deposition, very compact nanocomposite film was obtained , the nanorod arrays can not been seen in the SEM picture, which suggested the nanoscale interpenetrating structure between $CuInS_2$ nanocrystalls and TiO_2 nanorod array has formed. Energy dispersive spectroscopy (EDS) and EDS mapping equipped on SEM were employed to determine the composition of the nanostructure. In the spectrum (see the Supporting Information, SI-2), Ti and O peaks result from the TiO_2 nanorod array, and the ratio of Cu:In:S is 1:0.9:2 in the as-deposited chalcopyrite compounds.

The composition, structure, and interface character of the composite material were further characterized by TEM and HRTEM, the results were showed in Figure 3. Figure 3A,B shows a TEM and HRTEM image of a bare TiO_2 nanorod array, respectively, the distance of 0.316 nm between the adjacent lattice fringes is in agreement with the values for the (110) lattice planes of tetragonal rutile TiO_2. TEM image of $TiO_2/CuInS_2$ sample (Figure 3C) showed this $CuInS_2$ modified TiO_2 core−shell heterostructure clearly, from which we can see that the $CuInS_2$ nanocrystals directly anchored to the TiO2 nanorod surface. It can be further confirmed by the HRTEM image of Figure 3D. Parallel lattice planes appear in the image, the observed 0.308 nm lattice spacing can be assigned to the (112) planes of $CuInS_2$. The lattice of TiO_2 and $CuInS_2$ can be discriminated and are found to be in close contact, which is a key factor for fast electron inject from $CuInS_2$ to TiO_2.[27]

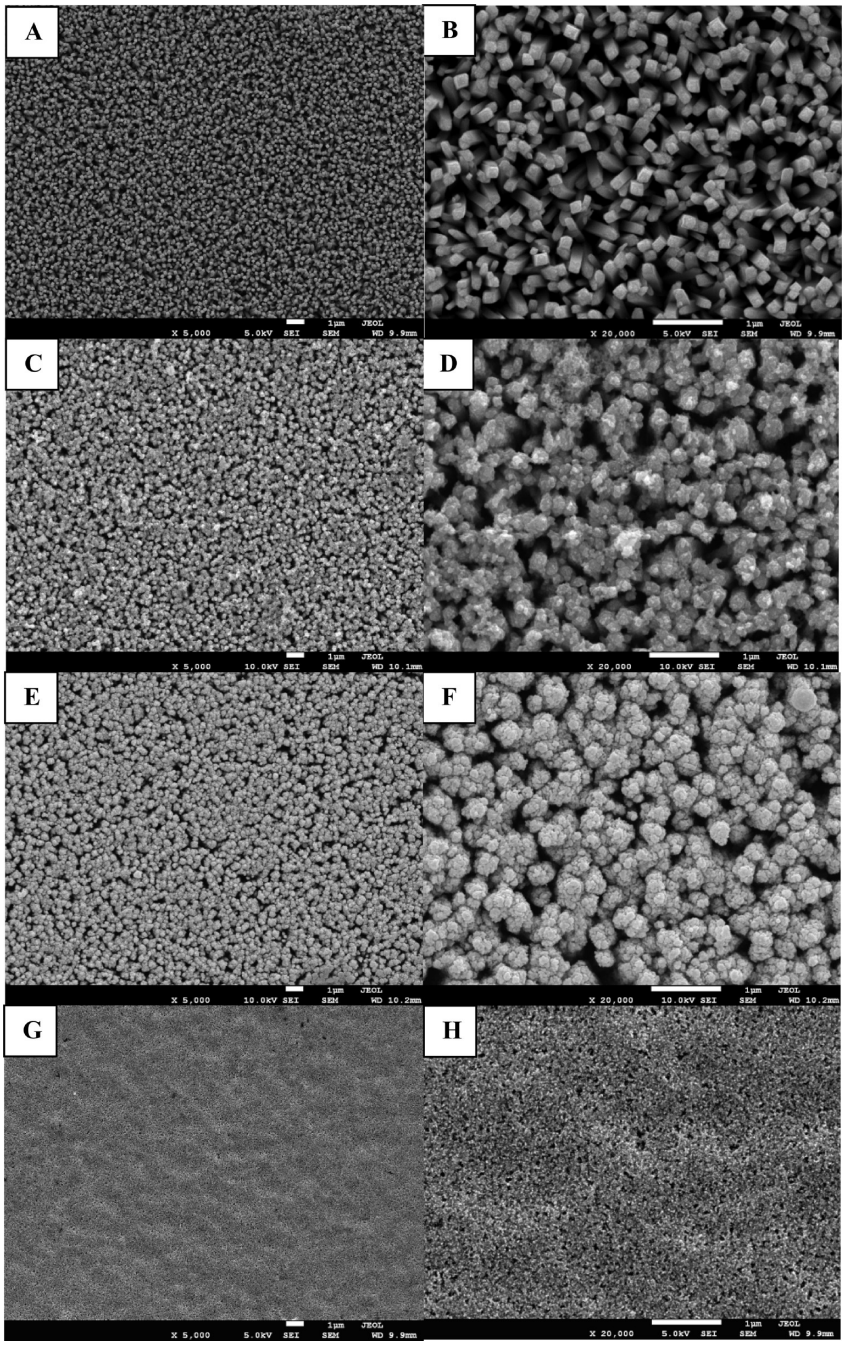

Figure 2. Field-emission scanning electron microscopy (FESEM) images of of FTO/TiO_2 and FTO/TiO_2/ $CuInS_2$ electrodes: typical top view SEM images of FTO/TiO_2 electrode at (A) high and(B) low magnifications; (C), (E, G) FTO/TiO_2/ $CuInS_2$ electrodes with $CuInS_2$ deposition for different cycles (5,10, and 20) by spin coating method; (D, F, H) corresponding high-magnification images of C, E, and G.

The crystal structure and phase composition of the products were characterized by X-ray diffractometry. Figure 4 shows XRD patterns of the FTO/TiO_2 and FTO/TiO_2/ $CuInS_2$ electrodes. Eliminating the peaks arising from the FTO conductive glass (Figure 4a), all the diffraction peaks that appear upon FTO/TiO_2 sample are attributed to the tetragonal rutile phase (JCPDS No.88-1175). The enhancement of (002) peak and absence of some peaks compared with polycrystalline or powder samples indicates that the nanorods are single crystalline throughout their length and grow in [001] direction with the growth axis perpendicular to the FTO substrate. After deposition of $CuInS_2$ nanocrystals, additional three peaks reflected from (1 1 2), (2 0 4)/(2 2 0), and (1 1 6)/(3 1 2) planes have appeared in the XRD pattern (Figure 4c), which matched well with the standard JCPDS-75-0106 pattern of tetragonal $CuInS_2$.

3.2. Optical and Photovoltage Properties of $CuInS_2$ Nanocrystals -Sensitized TiO_2 Nanorod Array. It is valuable to study the light absorption properties of the photoanode for application in photovoltaic device. Diffuse reflectance absorption spectra of FTO/TiO_2 electrode and FTO/TiO_2/$CuInS_2$ electrodes with different $CuInS_2$ nanocrystals coating cycles were compared in Figure 5. Barely FTO/TiO_2 electrode can only absorb ultraviolet

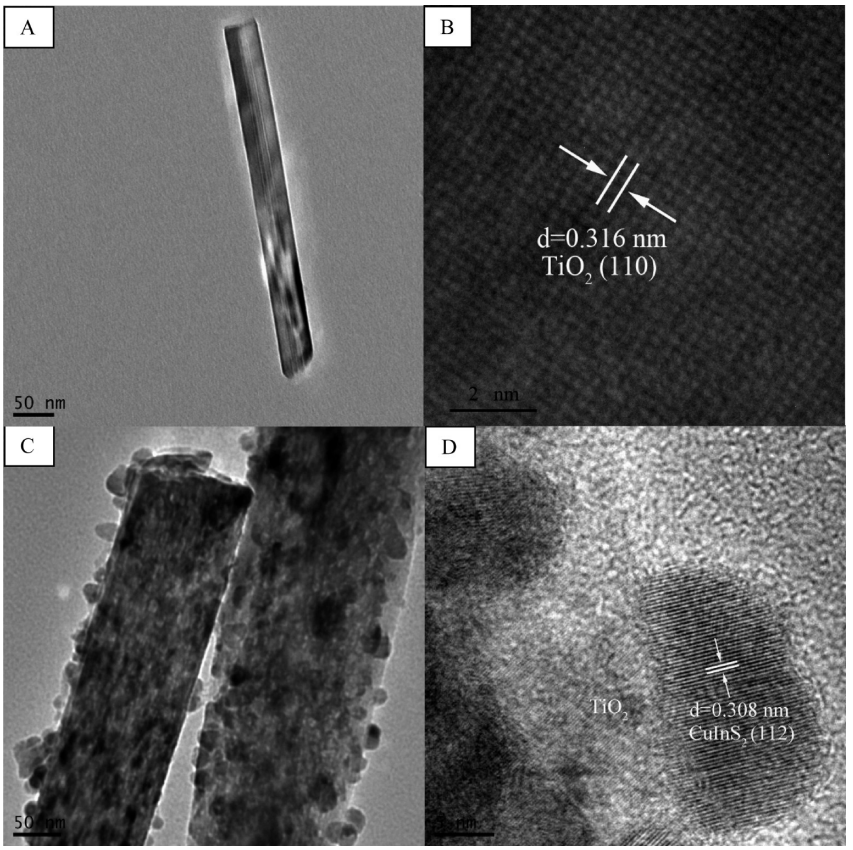

Figure 3. (A) TEM and (B) HRTEM image of the single bare TiO_2 nanorod. (C, D) TEM image and the corresponding HRTEM image of $CuInS_2$/TiO_2.

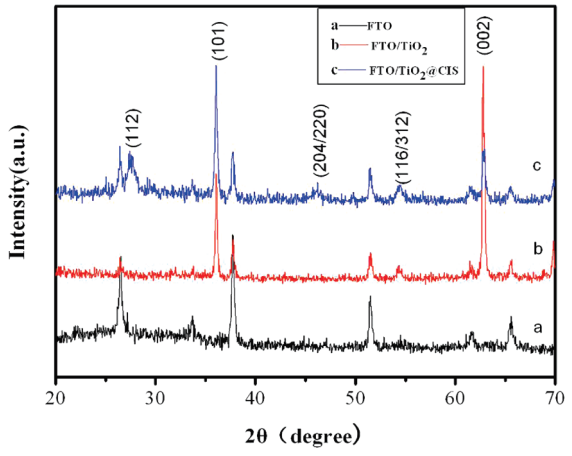

Figure 4. XRD pattern of (a) FTO, (b) FTO/TiO_2, and (c) FTO/TiO_2/ $CuInS_2$ electrodes.

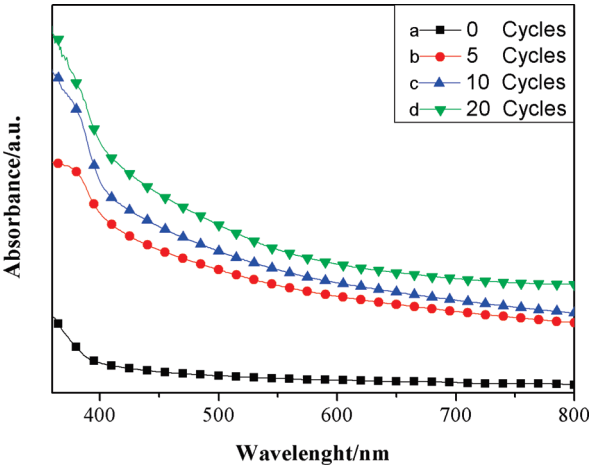

Figure 5. Diffuse reflectance absorption spectra of (a) FTO/TiO_2 photoelectrode and (b—d) FTO/TiO_2/$CuInS_2$ photoelectrodes with $CuInS_2$ deposition for (b) five, (c) ten, and (d) twenty cycles.

light with wavelength smaller than 410 nm. However, when the $CuInS_2$ nanocrystals were introduced into the TiO_2 nanorod array, the light absorbance extends to visible light region from 400 to 800 nm, which is the characteristic absorption of $CuInS_2$. Figure 5 also illustrates that the light absorbance was enhanced with an increase in spin-cast cycles.

Surface photovoltage spectrum technique is an effectively way to study the process of photoinduced charge separation and transfer in the surface and interface.[37,38] SPS measurements were carried out with a solid-junction photovoltaic FTO/sample/FTO sandwich structure (see the Supporting Information, SI-3). Here, SPS was used to characterize the photoelectric conversion efficiency of the photoelectrodes, the result was shown in Figure 6. There is only a weak peak at 360 nm was observed for FTO/TiO_2 electrode, attributed to the charge transition from valence band to conduction band of TiO_2 under ultraviolet light illumination. The SPV response band edge at 415 nm corresponds the band gap of 2.99 eV, further suggested that the synthesized TiO_2 is typical rutile phase.

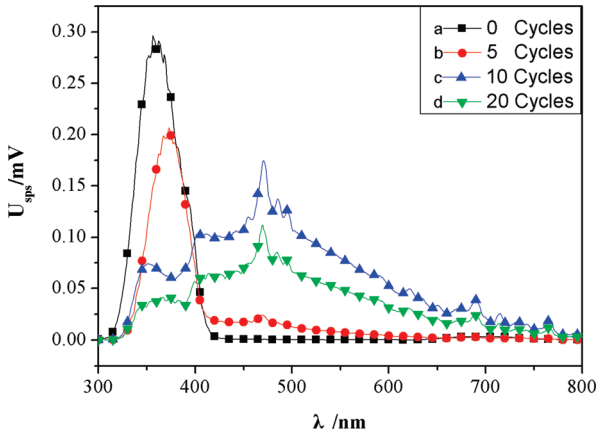

Figure 6. Surface photovoltage spectra of (a) bare TiO_2 nanorods array photoelectrode and (b–d) FTO/TiO_2/$CuInS_2$ photoelectrodes with $CuInS_2$ deposition for (b) 5, (c) 10, and (d) 20 cycles, respectively.

The SPS signal of FTO/TiO_2/$CuInS_2$ photoelectrodes was enhanced significantly compared with FTO/TiO_2 at the visible region (Figure 6), which shows that after deposition of $CuInS_2$ nanocrystals, the light response region of the composite photoelectrodes was extended to the visible band. The result is consistent with the absorption spectrum. From Figure 6, we can also see that with an increase in spin-coating cycles, the photovoltage response increased in visible light, indicating an increased deposition amount of $CuInS_2$. However, the SPS was weakened when the deposition circle continued for 20 cycles, this is mainly because excessive $CuInS_2$ lay over the surface of TiO_2 nanorod array, which will prevent the photogenerated electrons from $CuInS_2$ fast injecting into TiO_2 nanorods, resulting in the decrease of the photoelectrical properties.[39]

To acquire a better perspective on the sensitized enhancement mechanism of the photoelectrode heterostructure, the photogenerated electrons transfer process between interface of $CuInS_2$ and TiO_2 have been elucidated (see the Supporting Information, SI-4). In the as-prepared $CuInS_2$/TiO_2 assemblies, they form a type II heterojunction, both the valence and the conduction bands in $CuInS_2$ are higher than those in the TiO_2. Therefore, when the light harvesting $CuInS_2$ was excited, conduction-band electons are capable of injecting photogenerated electrons from the sensitizer into TiO_2 drived by the energy levels difference between the two conduction bands edges.[10,40,41] The excellen contact between $CuInS_2$ and TiO_2, which was evidenced by HRTEM, has ensured the fast electron transfer across the interface. At the same time, single-crystalline TiO_2 nanorods, which have superior electron separation and transport properties,[39] serves as an electron transport medium. The photoexcited electron finally decreases its energy by transferring along the TiO_2 nanorod to the collected FTO substrate.

The UV–visible absorption spectroscopy and SPS demonstrates that the novel photoelectrode of FTO/TiO_2 nanorod array/$CuInS_2$ possessed favorable optical and photovoltaic properties. It can be further used to assemble an all-solid-state solar cell and optimize through addition of appropriate buffer layer (such as In_2S_3), these investigations are in progress.

4. CONCLUSIONS

In summary, a simple solution method was developed for interpenetrating of $CuInS_2$ nanocrystals into the interspace of the TiO_2 nanorod matrix, and the optical and photovoltage properties of the novel photoelectrodes were investigated. The nanocomposite bulk heterojunction of p-type $CuInS_2$ and n-type TiO_2 displayed preferable visible light absorption ability and photogenerated charge separation and transport performance. The effect of different $CuInS_2$ deposition cycles on the photovoltaic performance of TiO_2/$CuInS_2$ hetero-interface structure has also been studied. Considering the present solution-processed synthesis route is facile and low-cost, we believe such a method would provide us a promising means for fabricating inorganic solid-state solar cell.

■ ASSOCIATED CONTENT

Supporting Information. SEM images of cross-sectional view of the well-aligned TiO_2 nanorod array before and after deposition of $CuInS_2$ nanocrystals, SEM–EDS and SEM-EDS elemental mapping of the $CuInS_2$/TiO_2 assembly, schematic diagram of SPS measurement with a solid-junction photovoltaic cell, and schematic showing the photogenerated electrons separation and transport process at the interface. This material is available free of charge via the Internet at http://pubs.acs.org.

■ AUTHOR INFORMATION

Corresponding Author
*E-mail: wusixin@henu.edu.cn.

■ ACKNOWLEDGMENT

This project is supported by the National Natural Science Foundation of China (20871041 and 20903033) and the New Century Excellent Talents in University (NCET-08-0659)

■ REFERENCES

(1) Fujishima, A.; Honda, K. *Nature* **1972**, *238*, 37–38.
(2) Wilson, J. M.; Idriss, H. *J. Am. Chem. Soc.* **2002**, *124*, 11284–11285.
(3) Robel, I.; Subramanian, V.; Kuno, M.; Kamat, P. V.; Yu, P. Y. *J. Am. Chem. Soc.* **2006**, *128*, 2385–2393.
(4) Wang, K. P.; Teng, H. *Appl. Phys. Lett.* **2007**, *91*, 173102–173105.
(5) Chuangchote, S.; Jitputti, J.; Sagawa, T.; Yoshikawa, S. *ACS Appl. Mater. Interfaces* **2009**, *1*, 1140–1143.
(6) Lee, H. J.; Leventis, H. C.; Moon, S. J.; Chen, P.; Ito, S.; Haque, S. A.; Torres, T.; Nuesch, F.; Geiger, T.; Zakeeruddin, S. M.; Grätzel, M.; Nazeeruddin, M. K. *Adv. Funct. Mater.* **2009**, *19*, 2735–2742.
(7) Costacurta, S.; Maso, G. D.; Gallo, R.; Guglielmi, M.; Brusatin, G.; Falcaro, P. *ACS Appl. Mater. Interfaces* **2010**, *2*, 1294–1298.
(8) Linsebigler, A. L.; Lu, G. Q.; Yates, J. T., Jr. *Chem. Rev.* **1995**, *95*, 735–758.
(9) Chen, X. B.; Mao, S. S. *Chem. Rev.* **2007**, *107*, 2891–2959.
(10) Li, T. L.; Lee, Y. L.; Teng, H. *J. Mater. Chem.* **2011**, *21*, 5089–5098.
(11) O'Regan, B.; Gratzel, M. *Nature* **1991**, *353*, 737–740.
(12) Mor, G. K.; Shankar, K.; Paulose, M.; Varghese, O. K.; Grimes, C. A. *Nano Lett.* **2006**, *6*, 215–218.
(13) Kongkanand, A.; Tvrdy, K.; Takechi, K.; Kuno, M. K.; Kamat, P. V. *J. Am. Chem. Soc.* **2008**, *130*, 4007–4015.
(14) Shooshtari, L.; Rahman, M.; Tajabadi, F.; Taghavinia, N. *ACS Appl. Mater. Interfaces* **2011**, *3*, 638–641.
(15) Hoyer, P.; Könenkamp, R. *Appl. Phys. Lett.* **1995**, *66*, 349–351.
(16) Hwang, J. Y.; Lee, S. A.; Lee, Y. H.; Seok, S. I. *ACS Appl. Mater. Interfaces* **2010**, *2*, 1343–1348.

(17) Okur, H. I.; Türker, Y.; Dag, O. *Langmuir* **2010**, *26*, 538–544.
(18) Kang, Q.; Liu, S. H.; Yang, L. X.; Cai, Q. Y.; Grimes, C. A. *ACS Appl. Mater. Interfaces* **2011**, *3*, 746–749.
(19) Larramona, G.; Choné, C.; Jacob, A.; Sakakura, D.; Delatouche, B.; Péré, D.; Cieren, X.; Nagino, M.; Bayón, R. *Chem. Mater.* **2006**, *18*, 1688–1696.
(20) Ning, Z. J.; Tian, H. N.; Yuan, C. Z.; Fu, Y.; Qin, H. Y.; Sun, L. C.; Agren, H. *Chem. Commun.* **2011**, *47*, 1536–1538.
(21) Sun, W. T.; Yu, Y.; Pan, H. Y.; Gao, X. F.; Chen, Q.; Peng, L. M. *J. Am. Chem. Soc.* **2008**, *130*, 1124–1125.
(22) Baker, D. R.; Kamat, P. V. *Adv. Funct. Mater.* **2009**, *19*, 805–811.
(23) Xie, Y.; Ali, G.; Yoo, S. H.; Cho, S. O. *ACS Appl. Mater. Interfaces* **2010**, *2*, 2910–2914.
(24) Tell, B.; Shay, J. L.; Kasper, H. M. *Phys. Rev. B* **1971**, *4*, 2463–2471.
(25) Contreras, M. A.; Ramanathan, K.; AbuShama, J.; Hasoon, F.; Young, D. L.; Egaas, B.; Noufi, R. *Prog. Photovoltaics* **2005**, *13*, 209–216.
(26) Park, G. C.; Chung, H. D.; Kim, C. D.; Park, H. R.; Jeong, W. J.; Kim, J. U.; Lee, K. H. *Sol. Energy Mater. Sol. Cells* **1997**, *49*, 365–374.
(27) Nanu, M.; Schoonman, J.; Goossens, A. *Adv. Mater.* **2003**, *16*, 453–456.
(28) Nanu, M.; Schoonman, J.; Goossens, A. *Nano Lett.* **2005**, *5*, 1716–1719.
(29) O'Hayre, R.; Nanu, M.; Schoonman, J.; Goossens, A.; Wang, Q.; Gr̈atzel, M. *Adv. Funct. Mater.* **2006**, *16*, 1566–1576.
(30) O'Hayre, R.; Nanu, M.; Schoonman, J.; Goossens, A. *Nanotechnology* **2007**, *18*, 055702–055708.
(31) Banerjee, S.; Mohapatra, S. K.; Das, P. P.; Misra, M. *Chem. Mater.* **2008**, *20*, 6784–6791.
(32) David, R. B.; Prashant, V. K. *Adv. Funct. Mater.* **2009**, *19*, 805–811.
(33) Tan, L. K.; Kumar, M. K.; An, W. W.; Gao, H. *ACS Appl. Mater. Interfaces* **2010**, *2*, 498–503.
(34) Yang, S. Y.; Nair, A. S.; Jose, R.; Ramakrishna, S. *Energy Environ. Sci.* **2010**, *3*, 2010–2014.
(35) Liu, B.; Aydil, E. S. *J. Am. Chem. Soc.* **2009**, *131*, 3985–3990.
(36) Li, L.; Coates, N.; Moses, D. *J. Am. Chem. Soc.* **2010**, *132*, 22–23.
(37) Lenzmann, F.; Krueger, J.; Brooks, S. *J. Phys. Chem. B* **2001**, *105*, 6347–6352.
(38) Cheng, K.; He, Y. P.; Miao, Y. M.; Zou, B. S.; Wang, Y. G.; Wang, T. H.; Zhang, X. T.; Du, Z. L. *J. Phys. Chem. B* **2006**, *110*, 7259–7264.
(39) Wang, H.; Bai, Y. S.; Zhang, H.; Zhang, Z. H.; Li, J. H.; Guo, L. *J. Phys. Chem. C* **2010**, *114*, 16451–16455.
(40) Li, T. L.; Teng, H. *J. Mater. Chem.* **2010**, *20*, 3656–3664.
(41) Medina-Gonzalez, Y.; Xu, W. Z.; Chen, B.; Farhanghi, N.; Charpentier, P. A. *Nanotechnology* **2011**, *22*, 065603–065610.